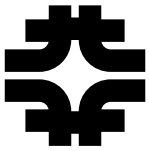

Fermi National Accelerator Laboratory

FERMILAB-Pub-96/270-E
CDF

Observation of $\Lambda_b^0 \rightarrow$ J/$\psi\Lambda$ at the Fermilab Proton-Antiproton Collider

F. Abe et al.
The CDF Collaboration

Fermi National Accelerator Laboratory
P.O. Box 500, Batavia, Illinois 60510

September 1996

Submitted to *Physical Review D*

Operated by Universities Research Association Inc. under Contract No. DE-AC02-76CHO3000 with the United States Department of Energy

Disclaimer

Distribution

CDF/PUB/BOTTOM/PUBLIC/3724
Version 3
August 27, 1996

Observation of $\Lambda_b^0 \to J/\psi\Lambda$ at the Fermilab Proton-Antiproton Collider

F. Abe,[15] H. Akimoto,[34] A. Akopian,[29] M. G. Albrow,[7] S. R. Amendolia,[25] D. Amidei,[18] J. Antos,[31] C. Anway-Wiese,[4] S. Aota,[34] G. Apollinari,[29] T. Asakawa,[34] W. Ashmanskas,[16] M. Atac,[7] F. Azfar,[24] P. Azzi-Bacchetta,[23] N. Bacchetta,[23] W. Badgett,[18] S. Bagdasarov,[29] M. W. Bailey,[20] J. Bao,[37] P. de Barbaro,[28] A. Barbaro-Galtieri,[16] V. E. Barnes,[27] B. A. Barnett,[14] E. Barzi,[8] G. Bauer,[17] T. Baumann,[10] F. Bedeschi,[25] S. Behrends,[3] S. Belforte,[25] G. Bellettini,[25] J. Bellinger,[36] D. Benjamin,[33] J. Benlloch,[17] J. Bensinger,[3] D. Benton,[24] A. Beretvas,[7] J. P. Berge,[7] J. Berryhill,[5] S. Bertolucci,[8] B. Bevensee,[24] A. Bhatti,[29] K. Biery,[13] M. Binkley,[7] D. Bisello,[23] R. E. Blair,[1] C. Blocker,[3] A. Bodek,[28] W. Bokhari,[17] V. Bolognesi,[2] G. Bolla,[23] D. Bortoletto,[27] J. Boudreau,[26] L. Breccia,[2] C. Bromberg,[19] N. Bruner,[20] E. Buckley-Geer,[7] H. S. Budd,[28] K. Burkett,[18] G. Busetto,[23] A. Byon-Wagner,[7] K. L. Byrum,[1] J. Cammerata,[14] C. Campagnari,[7] M. Campbell,[18] A. Caner,[25] W. Carithers,[16] D. Carlsmith,[36] A. Castro,[23] D. Cauz,[25] Y. Cen,[28] F. Cervelli,[25] P. S. Chang,[31] P. T. Chang,[31] H. Y. Chao,[31] J. Chapman,[18] M. -T. Cheng,[31] G. Chiarelli,[25] T. Chikamatsu,[34] C. N. Chiou,[31] L. Christofek,[12] S. Cihangir,[7] A. G. Clark,[9] M. Cobal,[25] E. Cocca,[25] M. Contreras,[5] J. Conway,[30] J. Cooper,[7] M. Cordelli,[8] C. Couyoumtzelis,[9] D. Crane,[1] D. Cronin-Hennessy,[6] R. Culbertson,[5] T. Daniels,[17] F. DeJongh,[7] S. Delchamps,[7] S. Dell'Agnello,[25] M. Dell'Orso,[25] R. Demina,[7] L. Demortier,[29] B. Denby,[25] M. Deninno,[2] P. F. Derwent,[7] T. Devlin,[30] J. R. Dittmann,[6] S. Donati,[25] J. Done,[32] T. Dorigo,[23] A. Dunn,[18] N. Eddy,[18] K. Einsweiler,[16] J. E. Elias,[7] R. Ely,[16] E. Engels, Jr.,[26] D. Errede,[12] S. Errede,[12] Q. Fan,[27] C. Ferretti,[25] I. Fiori,[2] B. Flaugher,[7] G. W. Foster,[7] M. Franklin,[10] M. Frautschi,[33] J. Freeman,[7] J. Friedman,[17] T. A. Fuess,[1] Y. Fukui,[15] S. Funaki,[34] G. Gagliardi,[25] S. Galeotti,[25] M. Gallinaro,[23] M. Garcia-Sciveres,[16] A. F. Garfinkel,[27] C. Gay,[10] S. Geer,[7] D. W. Gerdes,[14] P. Giannetti,[25] N. Giokaris,[29] P. Giromini,[8] G. Giusti,[25] L. Gladney,[24] D. Glenzinski,[14] M. Gold,[20] J. Gonzalez,[24] A. Gordon,[10] A. T. Goshaw,[6] K. Goulianos,[29] H. Grassmann,[25] L. Groer,[30] C. Grosso-Pilcher,[5] G. Guillian,[18] R. S. Guo,[31] C. Haber,[16] E. Hafen,[17] S. R. Hahn,[7] R. Hamilton,[10] R. Handler,[36] R. M. Hans,[37] K. Hara,[34] A. D. Hardman,[27] B. Harral,[24] R. M. Harris,[7] S. A. Hauger,[6] J. Hauser,[4] C. Hawk,[30] E. Hayashi,[34] J. Heinrich,[24] K. D. Hoffman,[27] M. Hohlmann,[5] C. Holck,[24] R. Hollebeek,[24] L. Holloway,[12] A. Hölscher,[13] S. Hong,[18] G. Houk,[24] P. Hu,[26] B. T. Huffman,[26] R. Hughes,[21] J. Huston,[19] J. Huth,[10] J. Hylen,[7] H. Ikeda,[34] M. Incagli,[25] J. Incandela,[7] G. Introzzi,[25] J. Iwai,[34] Y. Iwata,[11] H. Jensen,[7] U. Joshi,[7] R. W. Kadel,[16] E. Kajfasz,[23] H. Kambara,[9]

T. Kamon,[32] T. Kaneko,[34] K. Karr,[35] H. Kasha,[37] Y. Kato,[22] T. A. Keaffaber,[27] L. Keeble,[8] K. Kelley,[17] R. D. Kennedy,[30] R. Kephart,[7] P. Kesten,[16] D. Kestenbaum,[10] R. M. Keup,[12] H. Keutelian,[7] F. Keyvan,[4] B. Kharadia,[12] B. J. Kim,[28] D. H. Kim,[7a] H. S. Kim,[13] S. B. Kim,[18] S. H. Kim,[34] Y. K. Kim,[16] L. Kirsch,[3] P. Koehn,[28] K. Kondo,[34] J. Konigsberg,[10] S. Kopp,[5] K. Kordas,[13] A. Korytov,[17] W. Koska,[7] E. Kovacs,[7a] W. Kowald,[6] M. Krasberg,[18] J. Kroll,[7] M. Kruse,[28] T. Kuwabara,[34] S. E. Kuhlmann,[1] E. Kuns,[30] A. T. Laasanen,[27] N. Labanca,[25] S. Lammel,[7] J. I. Lamoureux,[3] T. LeCompte,[1] S. Leone,[25] J. D. Lewis,[7] P. Limon,[7] M. Lindgren,[4] T. M. Liss,[12] N. Lockyer,[24] O. Long,[24] C. Loomis,[30] M. Loreti,[23] J. Lu,[32] D. Lucchesi,[25] P. Lukens,[7] S. Lusin,[36] J. Lys,[16] K. Maeshima,[7] A. Maghakian,[29] P. Maksimovic,[17] M. Mangano,[25] J. Mansour,[19] M. Mariotti,[23] J. P. Marriner,[7] A. Martin,[12] J. A. J. Matthews,[20] R. Mattingly,[17] P. McIntyre,[32] P. Melese,[29] A. Menzione,[25] E. Meschi,[25] S. Metzler,[24] C. Miao,[18] T. Miao,[7] G. Michail,[10] R. Miller,[19] H. Minato,[34] S. Miscetti,[8] M. Mishina,[15] H. Mitsushio,[34] T. Miyamoto,[34] S. Miyashita,[34] N. Moggi,[25] Y. Morita,[15] J. Mueller,[26] A. Mukherjee,[7] T. Muller,[4] P. Murat,[25] H. Nakada,[34] I. Nakano,[34] C. Nelson,[7] D. Neuberger,[4] C. Newman-Holmes,[7] M. Ninomiya,[34] L. Nodulman,[1] S. H. Oh,[6] K. E. Ohl,[37] T. Ohmoto,[11] T. Ohsugi,[11] R. Oishi,[34] M. Okabe,[34] T. Okusawa,[22] R. Oliveira,[24] J. Olsen,[36] C. Pagliarone,[2] R. Paoletti,[25] V. Papadimitriou,[33] S. P. Pappas,[37] S. Park,[7] A. Parri,[8] J. Patrick,[7] G. Pauletta,[25] M. Paulini,[16] A. Perazzo,[25] L. Pescara,[23] M. D. Peters,[16] T. J. Phillips,[6] G. Piacentino,[2] M. Pillai,[28] K. T. Pitts,[7] R. Plunkett,[7] L. Pondrom,[36] J. Proudfoot,[1] F. Ptohos,[10] G. Punzi,[25] K. Ragan,[13] D. Reher,[16] A. Ribon,[23] F. Rimondi,[2] L. Ristori,[25] W. J. Robertson,[6] T. Rodrigo,[25] S. Rolli,[25] J. Romano,[5] L. Rosenson,[17] R. Roser,[12] W. K. Sakumoto,[28] D. Saltzberg,[5] A. Sansoni,[8] L. Santi,[25] H. Sato,[34] P. Schlabach,[7] E. E. Schmidt,[7] M. P. Schmidt,[37] A. Scribano,[25] S. Segler,[7] S. Seidel,[20] Y. Seiya,[34] G. Sganos,[13] M. D. Shapiro,[16] N. M. Shaw,[27] Q. Shen,[27] P. F. Shepard,[26] M. Shimojima,[34] M. Shochet,[5] J. Siegrist,[16] A. Sill,[33] P. Sinervo,[13] P. Singh,[26] J. Skarha,[14] K. Sliwa,[35] F. D. Snider,[14] T. Song,[18] J. Spalding,[7] T. Speer,[9] P. Sphicas,[17] F. Spinella,[25] M. Spiropulu,[10] L. Spiegel,[7] L. Stanco,[23] J. Steele,[36] A. Stefanini,[25] K. Strahl,[13] J. Strait,[7] R. Ströhmer,[7a] D. Stuart,[7] G. Sullivan,[5] A. Soumarokov,[31] K. Sumorok,[17] J. Suzuki,[34] T. Takada,[34] T. Takahashi,[22] T. Takano,[34] K. Takikawa,[34] N. Tamura,[11] F. Tartarelli,[25] W. Taylor,[13] P. K. Teng,[31] Y. Teramoto,[22] S. Tether,[17] D. Theriot,[7] T. L. Thomas,[20] R. Thun,[18] M. Timko,[35] P. Tipton,[28] A. Titov,[29] S. Tkaczyk,[7] D. Toback,[5] K. Tollefson,[28] A. Tollestrup,[7] J. F. de Troconiz,[10] S. Truitt,[18] J. Tseng,[14] N. Turini,[25] T. Uchida,[34] N. Uemura,[34] F. Ukegawa,[24] G. Unal,[24] J. Valls,[7a] S. C. van den Brink,[26] S. Vejcik, III,[18] G. Velev,[25] R. Vidal,[7] M. Vondracek,[12] D. Vucinic,[17] R. G. Wagner,[1] R. L. Wagner,[7] J. Wahl,[5] N. Wallace,[25] C. Wang,[6] C. H. Wang,[31] J. Wang,[5] M. J. Wang,[31] Q. F. Wang,[29] A. Warburton,[13] T. Watts,[30] R. Webb,[32] C. Wei,[6] C. Wendt,[36] H. Wenzel,[16] W. C. Wester, III,[7] A. B. Wicklund,[1] E. Wicklund,[7] R. Wilkinson,[24] H. H. Williams,[24] P. Wilson,[5] B. L. Winer,[21] D. Winn,[18] D. Wolinski,[18] J. Wolinski,[19] S. Worm,[20] X. Wu,[9] J. Wyss,[23] A. Yagil,[7] W. Yao,[16] K. Yasuoka,[34] Y. Ye,[13] G. P. Yeh,[7] P. Yeh,[31] M. Yin,[6] J. Yoh,[7] C. Yosef,[19] T. Yoshida,[22] D. Yovanovitch,[7] I. Yu,[7] L. Yu,[20] J. C. Yun,[7] A. Zanetti,[25] F. Zetti,[25] L. Zhang,[36] W. Zhang,[24] and S. Zucchelli[2]

(CDF Collaboration)

[1] *Argonne National Laboratory, Argonne, Illinois 60439*

[2] *Istituto Nazionale di Fisica Nucleare, University of Bologna, I-40126 Bologna, Italy*

[3] *Brandeis University, Waltham, Massachusetts 02254*

[4] *University of California at Los Angeles, Los Angeles, California 90024*

[5] *University of Chicago, Chicago, Illinois 60637*

[6] *Duke University, Durham, North Carolina 27708*

[7] *Fermi National Accelerator Laboratory, Batavia, Illinois 60510*

[8] *Laboratori Nazionali di Frascati, Istituto Nazionale di Fisica Nucleare, I-00044 Frascati, Italy*

[9] *University of Geneva, CH-1211 Geneva 4, Switzerland*

[10] *Harvard University, Cambridge, Massachusetts 02138*

[11] *Hiroshima University, Higashi-Hiroshima 724, Japan*

[12] *University of Illinois, Urbana, Illinois 61801*

[13] *Institute of Particle Physics, McGill University, Montreal H3A 2T8, and University of Toronto, Toronto M5S 1A7, Canada*

[14] *The Johns Hopkins University, Baltimore, Maryland 21218*

[15] *National Laboratory for High Energy Physics (KEK), Tsukuba, Ibaraki 305, Japan*

[16] *Ernest Orlando Lawrence Berkeley National Laboratory, Berkeley, California 94720*

[17] *Massachusetts Institute of Technology, Cambridge, Massachusetts 02139*

[18] *University of Michigan, Ann Arbor, Michigan 48109*

[19] *Michigan State University, East Lansing, Michigan 48824*

[20] *University of New Mexico, Albuquerque, New Mexico 87131*

[21] *The Ohio State University, Columbus, OH 43210*

[22] *Osaka City University, Osaka 588, Japan*

[23] *Universita di Padova, Istituto Nazionale di Fisica Nucleare, Sezione di Padova, I-35131 Padova, Italy*

[24] *University of Pennsylvania, Philadelphia, Pennsylvania 19104*

[25] *Istituto Nazionale di Fisica Nucleare, University and Scuola Normale Superiore of Pisa, I-56100 Pisa, Italy*

[26] *University of Pittsburgh, Pittsburgh, Pennsylvania 15260*

[27] *Purdue University, West Lafayette, Indiana 47907*

[28] *University of Rochester, Rochester, New York 14627*

[29] *Rockefeller University, New York, New York 10021*

[30] *Rutgers University, Piscataway, New Jersey 08854*

[31] *Academia Sinica, Taipei, Taiwan 11529, Republic of China*

[32] *Texas A&M University, College Station, Texas 77843*

[33] *Texas Tech University, Lubbock, Texas 79409*

[34] *University of Tsukuba, Tsukuba, Ibaraki 305, Japan*

[35] *Tufts University, Medford, Massachusetts 02155*

[36] *University of Wisconsin, Madison, Wisconsin 53706*

[37] *Yale University, New Haven, Connecticut 06511*

Abstract

The decay $\Lambda_b^0 \to J/\psi\Lambda$ is observed in 110 pb^{-1} of $p\overline{p}$ collisions taken at $\sqrt{s} = 1.8$ TeV. These data are used to measure a Λ_b^0 mass of $5621 \pm 4(stat.) \pm 3(sys.)$ MeV/c^2, and a mass difference between the Λ_b^0 and the B^0 of $340 \pm 5(stat.) \pm 1(sys.)$ MeV/c^2. The production cross section times branching fraction for the decay $\Lambda_b^0 \to J/\psi\Lambda$ relative to that for the decay $B^0 \to J/\psi K_S^0$ has been measured to be $0.27 \pm 0.12(stat.) \pm 0.05(sys.)$.

PACS Numbers: 14.20Mr, 13.30Eg, 13.85Ni

1 Introduction

Several recent results on B meson properties have been obtained with the Collider Detector at Fermilab (CDF) at the Tevatron $p\overline{p}$ Collider [1]. Masses, branching fractions, and lifetimes have been measured for fully reconstructed B^0, B^+, and B_s^0 decays with a J/ψ in the final state. This report extends the program of B hadron study into the baryon sector by the observation of the $\Lambda_b^0 \to J/\psi\Lambda$ decay [1]. The quark model predicts the existence of the Λ_b^0 baryon, a bound state of bottom, up, and down quarks, and calculations based on the non-relativistic heavy quark model predict the Λ_b^0 mass to fall within the range of $5600 - 5630$ MeV/c^2 [2]. The first claim of observation of the exclusive decay $\Lambda_b^0 \to J/\psi\Lambda$ came from the UA1 Collaboration at CERN [3] and was based on 16 ± 5 events. A branching fraction of $\mathcal{B}(\Lambda_b^0 \to J/\psi\Lambda) = (1.8 \pm 1.1) \times 10^{-2}$ was deduced by UA1, assuming 10% of the b quarks fragment to form the Λ_b^0. This result has been subsequently challenged by the inability of CDF and the LEP experiments to find the same resonance in this decay channel at the claimed production rate. In particular, a 2.6 pb^{-1} data sample collected by CDF in 1988-89 put an upper limit of $\mathcal{B}(\Lambda_b^0 \to J/\psi\Lambda) < 0.5 \times 10^{-2}$ at the 90% confidence level, also assuming that 10% of b quarks fragment to form the Λ_b [4].

Measurements of the Λ_b^0 lifetime have been obtained by CDF and several LEP experiments by exploiting the semileptonic decay channel $\Lambda_b^0 \to \Lambda_c^+ l\nu$ [5]. Unfortunately, the undetected neutrino in this decay channel does not allow for an accurate measurement of the Λ_b^0 mass. More recently, there have been reports that candidate Λ_b^0 events have been reconstructed by LEP experiments mainly in the channel $\Lambda_b^0 \to \Lambda_c^+\pi^-$ [6, 7]. This report describes the observation of the decays $\Lambda_b^0 \to J/\psi\Lambda, J/\psi \to \mu^+\mu^-, \Lambda \to p\pi^-$, the mass measurement of the Λ_b^0, and the measurement of the ratio of cross section times branching fraction, $\frac{\sigma_{\Lambda_b^0}\mathcal{B}(\Lambda_b^0 \to J/\psi\Lambda)}{\sigma_{B^0}\mathcal{B}(B_d^0 \to J/\psi K_S^0)}$, at CDF using a total of 110 pb^{-1} of integrated luminosity collected at $\sqrt{s} = 1.8$ TeV during 1992-95.

This report is organized in the following manner. Section 2 contains the detector description and event selection used for the reconstruction of the Λ_b^0 and reference signals. The masses of several reference signals used as a check on this analysis are presented in Section 3. We present our evidence for the observation of $\Lambda_b^0 \to J/\psi\Lambda$ in Section 4, along with the Λ_b^0 baryon mass measurement. Section 5 contains the measurement of the ratio of the cross section times branching fraction between the Λ_b^0 and B^0, and Section 6 contains our conclusions.

2 The Data Sample

2.1 Experiment

The CDF detector has been described in detail elsewhere [8, 9]. The charged tracks emerging from the $p\overline{p}$ interaction point are measured in a silicon vertex detector (SVX), a time projection chamber (VTX), and a central tracking chamber (CTC). All these tracking detectors are located in a 1.4 Tesla solenoidal field. Our standard coordinate system defines the z axis to be the proton beam direction, with ϕ and r being the azimuthal angle and transverse distance, respectively. The SVX consists of 4 layers of silicon strip detectors located outside the beam pipe at radii of 3.0, 4.2, 5.7, and 7.9 cm [10]. The strips are arranged axially, and have a pitch of 60 μm for the three innermost layers, and a pitch of 55 μm for

[1] Unless explicitly stated otherwise, the appearance of a specific charge state will also imply its charge conjugate throughout this paper.

the outer layer. The uncertainty in the track impact parameter ranges from 50 μm for tracks with transverse momentum $P_T = 1$ GeV/c to 15 μm for tracks with $P_T = 10$ GeV/c. The VTX provides $r - z$ information and is used in this analysis to determine the event vertex position in z. The CTC, an 84 layer drift chamber, covers the pseudorapidity interval $|\eta| < 1$ (where $\eta \equiv -\ln(\tan(\theta/2))$ and θ is the angle with respect to the proton beam direction) and provides information in both the $r - z$ and $r - \phi$ views. Efficiency for track reconstruction in the CTC cuts off for tracks with $P_T < 200$ MeV/c, rises over the range $200 < P_T < 400$ MeV/c, and is uniform for tracks with $P_T > 400$ MeV/c. The CTC also gives a measurement of the specific ionization of tracks that pass through it, providing some discrimination of particle type. This dE/dx system has been calibrated to provide a Gaussian distribution of measurements, so that particle selection can be made by requiring a maximum allowable deviation between actual and predicted ionization. The combined momentum resolution of the tracking chambers is $\delta P_T/P_T = [(0.0009 \times P_T)^2 + (0.0066)^2]^{1/2}$, with P_T measured in GeV/c.

Muons from the decay $J/\psi \rightarrow \mu^+\mu^-$ are identified by sets of drift chambers located outside the electromagnetic and hadron calorimeters at depths ranging from 5 to 8 interaction lengths. The central muon chambers (CMU) cover the region $|\eta| < 0.6$, and the central muon extension system continues this coverage to $|\eta| < 1.0$. These muon detectors are used in a three level trigger system to require a pair of muons in the event. The first level of trigger identifies muon candidates by requiring a coincidence between two radially aligned muon chambers. Two such coincidences are required for these data. The second level of the dimuon trigger combines the muon candidates with information from the fast track processor in the CTC. For the first 19.4 pb^{-1} of data collected, a single match between a muon chamber coincidence and a CTC track was required. The remainder of the data required two such matches, but with a lower requirement on the track P_T. The final level of the trigger was performed in software, and required events to contain oppositely charged muon candidate pairs with an invariant mass within 300 MeV/c^2 of the world average J/ψ mass of 3096.9 MeV/c^2 [11].

Charged particle track parameters of decay daughters are recalculated throughout this analysis by subjecting them to constrained fits, where the constraints are defined by the assumed decay process. The quality of each fit is measured by its χ^2, and we use a cut on $P_\nu(\chi^2)$, the cumulative probability of the constraint hypothesis for ν degrees of freedom, as our test for each fit. A requirement of $P_\nu(\chi^2) > 0.005$ is chosen for all constrained fits used in exclusive reconstructions.

2.2 Event Selection

The $J/\psi \rightarrow \mu^+\mu^-$ candidates are first selected by filtering events that contain two oppositely charged muon candidates with an invariant mass in the range $2800 - 3400$ MeV/c^2 after offline reconstruction. The match between the drift chamber track and the muon chamber track is required to be less than 3σ in the $r - \phi$ view and less than 3.5σ in the $r - z$ view for all muon candidates, where σ is the track extrapolation uncertainty due to resolution and multiple scattering. A minimum transverse momentum of 2.0 GeV/c is also required for each muon candidate to ensure that the muon trigger was efficient for the candidate dimuon events. In addition, events from the first 19.4 pb^{-1} of data required that at least one of the muon candidates have a transverse momentum above 2.8 GeV/c. The muon tracks are fit with a vertex constraint, which requires that they originate from a common point. Subsequently, a simultaneous mass and vertex constrained fit is performed, where the dimuon mass is constrained to

the J/ψ mass [11]. The dimuon invariant mass spectrum is shown in Figure 1.

The J/ψ sample is defined as the set of dimuons that satisfy the $P_\nu(\chi^2)$ cut on the combined vertex and mass constrained fit, and contains $\sim$ 416 000 events. We choose this definition, rather than the more standard approach of defining a mass window around the J/ψ, because it is more uniformly efficient over the range of J/ψ transverse momenta relevant for this analysis. We also identify a subset of the J/ψ sample by imposing a requirement on the precision of the dimuon flight distance with respect to the beamline. The flight distance of dimuons produced within the SVX acceptance is measured with far better precision than candidates with only drift chamber measurements, due to the precision of the vertex position measurement. This effect is illustrated in Figure 2. The flight distance uncertainty is required to be 250 μm or less for events we identify as having a precise vertex measurement. This sample contains $\sim$ 214 000 events, and is used for the branching fraction measurement.

2.3 Λ, K^0_S, and γ Selection

Events in the J/ψ data sample are searched for $\Lambda \to p\pi^-$ candidates. The mass assignments of the tracks used in the Λ search are made by assigning the proton mass to the track with the highest momentum. This mass assignment is always correct for the Λ's reconstructed in CDF due to the cutoff in acceptance at low transverse momenta. As a check on our reconstruction procedure, $K^0_S \to \pi^+\pi^-$ decays and conversion $\gamma \to e^+e^-$ candidates are identified as well. The oppositely charged track pairs are refit with a vertex constraint for the K^0_S and Λ candidates. Photons are identified by imposing the additional constraint of parallelism on the two tracks at their point of intersection.

Three requirements are imposed on these signals to reduce combinatoric backgrounds. A displacement of 1.0 cm or more with respect to the dimuon vertex in the direction of the neutral object's transverse momentum is required, which reduces the background due to tracks originating at the primary vertex. Also, consistency is required between the dE/dx measurement provided by the CTC for each track and the expected value for its mass assignment. Particle candidates are rejected if their measured specific ionization falls more than 2σ away from their predicted value. Finally, we require $P_T > 1.5$ GeV/c for K^0_S and Λ candidates, and $P_T > 1.0$ GeV/c for photon candidates. The $\pi^+\pi^-$ and π^-p invariant mass spectra, obtained after these requirements are imposed, are shown in Figures 3 and 4, respectively, and clearly demonstrate K^0_S and Λ signals. Invariant mass ranges of ± 12 MeV/c^2 and ± 4 MeV/c^2 around the world average masses of 497.67 MeV/c^2 and 1115.7 MeV/c^2 are used to define the K^0_S and Λ signal regions, respectively. A second constrained fit is then performed that simultaneously constrains the muon momenta to form the world average J/ψ mass [11], and the K^0_S, Λ or γ momentum to point to the dimuon vertex. All masses and momenta used for further cuts make use of the momenta calculated from this final constrained fit, and combinations with $P_T > 6.0$ GeV/c and $|\eta| < 1.0$ are retained for further study.

3 Reference Signals

3.1 Mass Measurement

The performance of the tracking system and the methods used in this analysis are tested on the accessible reference signals with a J/ψ or Λ in the final state to confirm that known

states can be reconstructed and their masses measured with accuracy. These signals are used as a check for possible systematic errors in the reconstruction. The mass of each reference signal is calculated by performing an unbinned likelihood fit on the data, where each event is weighted by the calculated uncertainty on its mass measurement. This fit involves maximizing the likelihood function

$$\mathcal{L} = \frac{e^{-(N_s+N_b)}}{N!} \prod_{i=1}^{N} \left[N_s \times \frac{e^{\frac{-(m_i-P_1)^2}{2(P_2\sigma_i)^2}}}{\sqrt{2\pi} \times P_2\sigma_i} + N_b(P_3 + P_4 \times m_i) \right], \quad (1)$$

where N_s and N_b are the number of signal and background events, which together with the P_n are the parameters of the fit, m_i and σ_i are the measured mass and mass uncertainty for each event, and N is the total number of events in the mass distribution. Binned fits are also performed on the mass distributions in Figures 5-9 and 12, but these are used soley for visualization purposes.

3.2 Reconstruction of ψ(2S)

The first reference signal uses the decay $\psi(2S) \to J/\psi\pi^+\pi^-$. Events are selected for this sample by making the minimal changes from the selection criteria used for the B hadron decays. We therefore use all combinations where the $\pi^+\pi^-$ invariant mass falls within the our K^0_S search range of $450 - 550$ MeV/c^2, and we make no requirement on the $\pi^+\pi^-$ flight distance. All other kinematic requirements are identical to those used for the K^0_S sample. This charmonium decay differs from $\Lambda^0_b \to J/\psi\Lambda$ reconstruction because both the pions and muons in the final state originate from the same point. We have used the $\psi(2S)$ as a check on the analysis method by treating the final state as having independent $\mu^+\mu^-$ and $\pi^+\pi^-$ vertices, and then performing the same set of constrained fits that are used for $\Lambda^0_b \to J/\psi\Lambda$ reconstruction. The resulting $J/\psi\pi^+\pi^-$ invariant mass distribution is shown in Figure 5. The reconstructed mass of 3686.1 $\pm$ 0.3 MeV/c^2 is consistent with the world average value of 3686.0 $\pm$ 0.1 MeV/c^2 [11]. This measurement demonstrates the ability of the experiment to accurately reconstruct a known state with relatively low momentum tracks.

3.3 Reconstruction of χ_{c1}(1P) and χ_{c2}(1P)

One limitation of the $\psi(2S)$ as a reference signal is that its "secondary" vertex is not displaced, so any systematic error due to displacement will not be tested. Candidate signals whose secondary vertices appear at a range of displacements from the beamline are the $\chi_{c1}(1P)$ and $\chi_{c2}(1P)$ decays into the $J/\psi\gamma$ final state, where the photon is reconstructed through its conversion to e^+e^-. These conversions originate in the tracking chamber material throughout an interval of $1.0 - 27.7$ cm transverse to the beamline. The $J/\psi\gamma$ invariant mass spectrum found is shown in Figure 6. This mass distribution is fit with a likelihood function that differs from Equation 1 by the addition of a second Gaussian signal term. The two Gaussians are constrained to have identical widths by fitting only one mass scale error parameter (P_2 in eq. (1)), and a mass difference equal to the world average difference between the $\chi_{c1}(1P)$ and $\chi_{c2}(1P)$ of 46.64 MeV/c^2 [11]. The mass measurements obtained for these charmonium states are 3510.7 $\pm$ 0.4 and 3556.3 $\pm$ 0.4 MeV/c^2, respectively, which are consistent with the world average values of 3510.5 $\pm$ 0.1 and 3556.2 $\pm$ 0.1 MeV/c^2 [11]. Consequently, the addition of the vertex displacement appears to have no deleterious effect on the mass measurement.

3.4 Reconstruction of Ξ^-

Final states that include the Λ baryon may suffer systematic errors unique to Λ reconstruction. The kinematics of the $\Lambda \to p\pi^-$ decay force an asymmetry between the proton and pion momenta for Λ's within the CDF acceptance ($P_T(\Lambda) > 1.0$ GeV/c). This feature may cause a charge dependent momentum mismeasurement of the Λ, and a corresponding error when the Λ candidate is subjected to a pointing constraint fit. The reconstruction of the $\Xi^- \to \Lambda\pi^-$ decay is used as a check on our ability to measure the Λ momentum. The technique used here differs from the fitting procedure used in the two charmonium decays, since no J/ψ is involved. Tracks in our J/ψ sample which are not identified as muons or Λ decay products are assigned the pion mass and combined with the Λ candidates in the Ξ^- search. The three tracks used are then refit with the constraints that the Λ decay daughters form the world average Λ mass [11], and the Λ and π^- trajectories intersect. Additional requirements are imposed on the Ξ^- candidates to reduce the combinatoric background. The transverse impact parameters of the Λ decay daughters with respect to the beamline are required to exceed their measurement uncertainties, the Ξ^- flight distance is required to be 2.0 cm or greater, and the Λ flight distance is required to exceed the Ξ^- flight distance by at least 1.0 cm. The $\Lambda\pi^-$ mass spectrum found with this procedure is shown in Figure 7. The sample is divided into the $\Lambda\pi^-$ and $\overline{\Lambda}\pi^+$ mass spectra, and these are shown as well. The mass spectra indicate clear signals for the Ξ^+ and Ξ^-, and the masses for these states are found to be 1321.8 ± 0.3 MeV/c^2 and 1321.6 ± 0.3 MeV/c^2, respectively. Each is found to be consistent with the world average value of 1321.3 ± 0.1 MeV/c^2 [11]. A simultaneous fit to the entire sample yields 1321.7 ± 0.3 MeV/c^2, where the uncertainties are statistical only. We conclude that we have no systematic problem with Λ baryon reconstruction.

3.5 Reconstruction of B^0

The reference signal most similar to the $\Lambda_b^0 \to J/\psi\Lambda$ is the decay $B^0 \to J/\psi K_S^0$. Simulation of these decays in our detector indicates the expected mass resolution is 13 ± 1 MeV/c^2 for both states. A lifetime requirement of $c\tau > 100$ μm is imposed on these B hadron states, which reduces the large background from direct charmonium production. The $J/\psi K_S^0$ invariant mass spectrum obtained is shown in Figure 8. The measured B^0 mass of 5281.3 ± 1.8 MeV/c^2 is consistent with the world average value of 5279.2 ± 1.8 MeV/c^2 [11], and the measured width is consistent with our expected mass resolution. As in the previous reference signals, the mass uncertainty on each event is used as the signal resolution in the likelihood function. A scale factor of 1.15 ± 0.18 is obtained from the fit (parameter P_2 from equation (1)), and establishes the accuracy of our mass uncertainty estimates.

A summary of mass measurements of the reference signals is included in Table I. These reference signals demonstrate the experiment's ability to reconstruct three different resonances with a J/ψ and a neutral vertex in the final state, and to make mass measurements of those states which are consistent with the world average values. Also, the successful reconstruction and mass measurement of the Ξ^- demonstrates that Λ's are unlikely to possess any anomalous traits that would make mass measurements involving Λ's unreliable.

Table I: Measured masses of reference signals and their deviation from the world average values [11] . The uncertainties shown are statistical only.

Signal	Mass (MeV/c^2)	Mass - Mass$_{PDG}$ (MeV/c^2)
$\psi(2S)$	3686.1$\pm$0.3	0.1 ± 0.3
$\chi(1P)/\chi(2P)$	3510.7/3556.3$\pm$0.4	0.2 ± 0.4
Ξ^-	1321.7$\pm$0.3	0.4 ± 0.3
B^0	5281.3$\pm$1.8	2.1 ± 2.5

4 Evidence for the Λ_b^0

The $J/\psi\Lambda$ invariant mass spectrum obtained after our Λ selection criteria and the $c\tau > 100\mu$m cut is shown in Figure 9. We have excluded π-p candidates from this distribution if a $\pi\pi$ mass assignment would yield an invariant mass consistent with K_S^0 decay. This requirement is imposed to avoid possible reflections from K_S^0 decay. It removes 15 events, uniformly distributed in invariant mass, from the mass region shown in Figure 9.

Given the expected mass resolution ($\sim$ 13 MeV/c^2), a mass window containing $\sim$ 90% of the Λ_b^0 candidates is 50 MeV/c^2 wide. In the 5 bins in the mass region $5600 - 5650$ MeV/c^2 we observe 38 events. The expected average number of background events in the same region is interpolated from a linear fit to the sidebands and is found to be 18.1 ± 1.6 events. The number of candidates in the signal region returned from the Gaussian part of the fit to this distribution is found to be 19.9 ± 6.4.

4.1 Statistical Significance

We estimate the probability that the linear background would fluctuate up to the number of observed events any place inside a given search window. Conservatively, we have chosen the whole mass range that we use for displaying the data ($5400 - 5800$ MeV/c^2) as our search window. Alternatively, we will also use a search window suggested by the measurements recently reported by ALEPH [6] and DELPHI [7] with mass determinations of $M_{\Lambda_b^0} = 5616 \pm 21(stat.) \pm 4(sys.)$ MeV/c^2 and $5668 \pm 16(stat.) \pm 8(sys.)$ MeV/c^2, respectively. Our expected mass resolution is convoluted with these recent mass measurements to define a window of $5540 \leq M_{\Lambda_b^0} \leq 5730$ MeV/c^2. We begin the significance test by generating a large number of simulated background mass spectra distributed according to the flat background we observe in our data. We then calculate the probability of observing 5 consecutive bins with the same number or more events than we observe in this data. The resulting probability that our Λ_b^0 signal is due to a background fluctuation is found to be 0.91% for the conservative search window, and 0.07% for the narrower window. These probabilities correspond to approximately 2.6σ and 3.4σ for a normal distribution. The statistical significance of the signal has also been tested for variations in the event selection requirements, and we find the signal to be robust. We conclude that the enhancement of events seen in the $J/\psi\Lambda$ mass spectrum is a signal for the Λ_b^0, and not a background fluctuation.

4.2 Λ_b^0 Mass Determination

When the excess of events near 5620 MeV/c^2 in the $J/\psi\Lambda$ invariant mass spectrum is interpreted as the Λ_b^0 , the unbinned likelihood fit to the mass distribution performed on the reference signals can be applied to the data displayed in Figure 9. Since the predicted mass resolutions of the B^0 and Λ_b^0 are identical, the mass uncertainty scale parameter (P_2 in eq. (1)) has been fixed in this $J/\psi\Lambda$ fit to the value obtained in the B^0 mass fit. This technique provides a Λ_b^0 mass measurement of $5621 \pm 4(stat.)$ MeV/c^2.

4.3 Systematic Uncertainties on the Mass Measurement

The systematic uncertainties on the Λ_b^0 mass measurement are very similar to the uncertainties on our earlier measurement of the mass of the B_s^0 [12, 13], yielding a similar estimate. The various components of the systematic uncertainty are detailed here.

The absolute value of the momentum scale in CDF is calibrated by normalizing the average reconstructed J/ψ mass to its world average value [11] as shown in Refs. [13, 14]. After this normalization there is a residual time dependent variation of 0.17% during the course of the experiment as measured by a set of NMR probes immersed in the CDF tracking volume. This variation is not removed from the data and remains as a systematic error. This full range of field variation corresponds to a mass variation of 2.6 MeV/c^2 for both the B^0 and Λ_b^0 mass measurements. We have chosen to take one half of this variation as representative of our systematic uncertainty due to the momentum scale.

The unbinned likelihood fit used for the Λ_b^0 mass determination uses the measured mass uncertainty for each event. This mass uncertainty is a function of the reconstructed track parameter uncertainties. These uncertainties can be miscalculated due to irregularities or lack of understanding of the material in the detector. In particular, we have determined that the scaling of the covariance matrix [13] required for consistency with other measured tracking uncertainties is due in large part to the effect of multiple scattering of the charged particles in the gas volume of the CTC. The track fitting procedure has been modified for the B^0 and Λ_b^0 candidates to include the effect of the multiple scattering in all known detector materials (including the gas in the tracking volume) and the individual masses are measured for the B^0 and Λ_b^0 candidates for a reasonable range of covariance scaling. A mass shift of 0.5 MeV/c^2 is seen when the covariance scaling is varied over a wide range, and this value is assigned as the systematic mass uncertainty due to the uncertainty in track parameter measurement.

Reconstructed tracks have their momentum measurements corrected for the energy loss due to passage through the material within the tracking system. This energy loss correction has the potential of introducing a systematic uncertainty due to the presence of a relatively slow moving proton in the Λ decay. The event by event mass differences for the Λ_b^0 candidates and the sideband events are studied when the energy loss correction is varied as shown in Ref. [13]. The average shift in mass is 0.6 MeV/c^2. This shift is taken as the systematic uncertainty on the mass measurement due to the energy loss correction.

A variation in the measured J/ψ mass as a function of the opening angle between the two muons in the longitudinal plane was noted in earlier mass measurements [13, 14]. This effect leads to a variation in the reconstructed B hadron mass. In Refs. [13, 14] this $\Delta\cot(\theta)$ effect is removed by scaling the $\cot(\theta)$ of the measured tracks by 0.9985 ± 0.0008. In this analysis, the impact of this effect is tested by measuring the mass variation, on an event by event basis,

of the Λ_b^0 and B^0 candidates before and after the scaling of $\cot(\theta)$. We use scale factors that cover the range $0.9977 - 1.0$. An average mass shift of 2.0 MeV/c^2 is found, and is taken as our systematic uncertainty for this effect.

Early B meson mass measurements from CDF [12] reported the presence of a false curvature effect. We employ the final tracking detector alignments used for the B_s^0 analysis [13]. These were shown to leave no statistically significant false curvature, so we treat this effect as also negligible in this analysis. In addition, the mass difference between the Ξ^+ and Ξ^- (section 5), which should depend heavily on such an effect, is only 0.2 MeV/c^2. Consequently, no systematic error on the mass measurement is attributed to this effect.

Table II: Systematic uncertainties in the Λ_b^0 Mass Measurement

Effect	Uncertainty (MeV/c^2)
Track Measurement	0.5
$\Delta cot(\theta)$	2.0
Momentum Scale	1.3
Energy Loss	0.6
Total	3.0

4.4 Mass Measurement Conclusion

A summary of the systematic uncertainties on the Λ_b^0 mass measurement appears in Table II. We have combined these in quadrature to obtain an overall systematic uncertainty of 3 MeV/c^2. As a check on this uncertainty, it can be noted that the same systematic uncertainty would be estimated for a B^0 mass measurement, and our measurement of that state is well within 3 MeV/c^2 of the world average value [11]. Moreover, the agreement between the masses of the reference signals examined in section 5 and the accepted values gives additional confidence that no other large source of systematic bias is present in the mass measurement. Consequently, our final value for the Λ_b^0 mass is $5621 \pm 4(stat.) \pm 3(sys.)$ MeV/c^2.

The systematic effects impact the mass measurements of both the B^0 and Λ_b^0 similarly, so a difference in their masses can be measured which is almost free of systematic errors. A Monte Carlo sample of events was used to verify that any change in the systematic effects studied here will introduce a shift in the mass difference of 1 MeV/c^2 or less. We take this as our systematic uncertainty, and find this difference to be $M_{\Lambda_b^0} - M_{B^0} = 340 \pm 5(stat.) \pm 1(sys.)$ MeV/c^2.

5 Measurement of $\frac{\sigma(p\overline{p}\to\Lambda_b^0 X)\mathcal{B}(\Lambda_b^0\to J/\psi\Lambda)}{\sigma(p\overline{p}\to B^0 X)\mathcal{B}(B^0\to J/\psi K_S^0)}$

A direct measurement of the Λ_b^0 cross section times branching fraction ($\sigma(p\overline{p} \to \Lambda_b^0)\mathcal{B}(\Lambda_b^0 \to J/\psi\Lambda)$) is possible with these data, but such a measurement will contain large systematic uncertainties. By measuring $\frac{\sigma(p\overline{p}\to\Lambda_b^0 X)\mathcal{B}(\Lambda_b^0\to J/\psi\Lambda)}{\sigma(p\overline{p}\to B^0 X)\mathcal{B}(B^0\to J/\psi K_S^0)}$ we minimize several systematic uncertainties, since they closely or completely cancel in this ratio. The largest of these uncertainties are associated with the b quark production cross section and transverse momentum spectrum. The ratio of production cross sections is computed using the relation

$$\frac{\sigma(p\overline{p}\to\Lambda_b^0 X)\mathcal{B}(\Lambda_b^0\to J/\psi\Lambda)\mathcal{B}(\Lambda\to p\pi)}{\sigma(p\overline{p}\to B^0 X)\mathcal{B}(B^0\to J/\psi K_S^0)\mathcal{B}(K_S^0\to\pi^+\pi^-)} = \frac{N_{\Lambda_b^0}}{N_{B^0}} \times \frac{\epsilon_{B^0}}{\epsilon_{\Lambda_b^0}},$$

where $\mathcal{B}(\Lambda \to p\pi) = 0.639 \pm 0.005$, $\mathcal{B}(B^0 \to J/\psi K_s^0) = (3.7 \pm 1.0) \times 10^{-4}$, $\mathcal{B}(K_s^0 \to \pi^+\pi^-) = 0.686 \pm 0.003$ [11], $N_{\Lambda_b^0}$ is the number of observed Λ_b^0 candidates, N_{B^0} is the number of observed B^0 mesons, $\epsilon_{\Lambda_b^0}$ is the overall efficiency of Λ_b^0 reconstruction, and ϵ_{B^0} is the overall efficiency of B^0 reconstruction.

5.1 Additional Requirements

Three additional requirements are imposed on the B^0 and Λ_b^0 samples for the rate measurement. All three are made to restrict the data so that efficiencies are well measured. While additional cuts have the effect of increasing the statistical uncertainty on the measurement, the systematic uncertainties on the measurement of the ratio of efficiencies are serious enough to warrant the decision.

Firstly, we have limited the sample to events with both muons reconstructed in the SVX by requiring the vertex measurement error selection discussed in section 2.2. The requirement on the hadron lifetime of $c\tau > 100$ μm will have a different efficiency for events measured in the SVX compared to events measured only in the drift chamber. By limiting the data sample to events with a well measured vertex position, we become less sensitive to the way in which the data is distributed along the beamline, and less sensitive to our simulation of the detector. Although the vertex precision requirement reduces the data sample by approximately a factor of 2, it has the effect of removing more background than signal so the statistical uncertainty due to this cut rises only slightly (from $\sim 30\%$ to $\sim 40\%$).

Secondly, we need to limit the data to a sample where the tracking efficiency is understood. Our charged particle reconstruction efficiency rises quickly in the range of transverse momentum from $200 - 400$ MeV/c, and overlaps with the P_T distribution of the daughter pions from our Λ sample, as shown in Figure 10. The exact shape and plateau of the efficiency is a strong function of both instantaneous and integrated luminosity, track density, and electric charge. A measurement of the Λ_b^0 rate in this region of nonuniform efficiency would require a detailed understanding of the efficiency function, an accurate estimate of the momentum distribution of decay pions from the Λ_b^0, and would introduce additional systematic uncertainty for the corrections. Consequently, the data have had a $P_T(\pi) > 400$ MeV/c cut imposed on them. This is the lowest transverse momentum with uniform tracking efficiency. While the absolute value of this efficiency has not been determined, its insensitivity to transverse momentum is checked by studying the decay angle distribution of the K_S^0 in this data. This decay angle Θ is defined as the angle between the π^+ momentum and the K_S^0 flight direction, as measured in the K_S^0 rest frame. Since the K_S^0 is a pseudoscalar particle, the distribution of $\cos(\Theta)$ should be uniform. Any deviation from uniformity indicates an inefficiency in tracking. The distribution of $\cos(\Theta)$ for events with $P_T(K_S^0) > 2$ GeV/c is shown in Figure 11. The $P_T(\pi) > 400$ MeV/c requirement is satisfied for decays of K_S^0 with $|\cos(\Theta)| < 0.7$ in this data, where the yield of K_S^0 is seen to be uniform. This cut on the minimum $P_T(\pi)$ has the effect of removing approximately 30% of the Λ_b^0 candidates.

Finally, we restrict the data to events that are triggered and reconstructed in the CMU system, where the trigger efficiency is well measured [15]. This cut is relatively minor, and

results in a loss of only three out of the 38 candidates in the Λ_b^0 mass region. This last requirement effectively restricts the Λ_b^0 candidates to the central region ($|\eta| < 0.6$).

5.2 Ratio of Efficiencies

The ratio of efficiencies for several of the selection requirements used for the search of the Λ_b^0 (i.e. χ^2 cuts) can be checked on the large Λ and K_S^0 inclusive samples, and is very close to unity, as expected. For the other cuts, we rely on a Monte Carlo simulation including a next-to-leading order QCD calculation [16] with renormalization scale $\mu_0^2 = (P_T^2 + m_b^2)$ (where the b-quark mass m_b was set to 4.75 GeV/c^2), the MRSD0 proton parton distribution function [17], the Peterson parametrization [18] for b-quark fragmentation with a value of the fragmentation parameter $\epsilon = 0.006$, and a detector and trigger simulation. The lifetimes used in the simulation were obtained from the recent measurement for the Λ_b^0 [5] and the world average value for the B^0 [11]. The final value for the ratio of efficiencies times the K_S^0 and Λ decay branching fractions is $\epsilon_{B^0}\mathcal{B}(K_S^0 \to \pi^+\pi^-)/\epsilon_{\Lambda_b^0}\mathcal{B}(\Lambda \to p\pi^-) = 2.02 \pm 0.05$. The relative softness of the π^-, and the $P_T(\pi^-) > 400$ MeV/c requirement are responsible for the lower efficiency in the $\Lambda \to p\pi^-$ reconstruction.

5.3 Measurement of $N_{\Lambda_b^0}/N_{B^0}$

Figure 12 shows the Λ_b^0 and B^0 candidates after the imposition of the three additional selection requirements made for the rate measurement. The unbinned likelihood fit of a Gaussian signal plus linear background gives us 7.8 ± 3.4 Λ_b^0 candidates and 57.6 ± 8.7 B^0 candidates. With these yields we obtain

$$\frac{\sigma(p\bar{p}\to\Lambda_b^0 X)\mathcal{B}(\Lambda_b^0\to J/\psi\Lambda)}{\sigma(p\bar{p}\to B^0 X)\mathcal{B}(B^0\to J/\psi K_S^0)} = 0.27 \pm 0.12(stat.).$$

5.4 Systematic Uncertainties on $\epsilon_{B^0}/\epsilon_{\Lambda_b^0}$

There are a number of parameters in the Monte Carlo that are not known exactly (theoretical uncertainties). Similarly, some experimental inputs (Λ_b^0 lifetime) or detector simulation parameters are known with limited precision. All these uncertainties can affect $\epsilon_{B^0}/\epsilon_{\Lambda_b^0}$ and therefore give rise to a systematic uncertainty.

The theoretical uncertainties are dominated by the unknown polarization and decay parameters of the Λ_b^0 and by the value of the Peterson fragmentation parameter ϵ for a baryon. The effect of the polarization and decay parameters of the Λ_b^0 on the efficiency ratio is studied following the formalism of Refs. [19, 20]. In particular, Θ, the emission angle of the Λ with respect to the polarization direction in the Λ_b^0 rest frame, follows the distribution $I(\Theta) \propto 1 \pm \alpha(\Lambda_b^0)P(\Lambda_b^0)\cos\Theta$, where $\alpha(\Lambda_b^0)$ and $P(\Lambda_b^0)$ are unknown. Wide ranges of possible values for $P(\Lambda_b^0)$ and the Λ_b^0 decay parameters have been used in the simulation, and we determine the largest variation in $\epsilon_{B^0}/\epsilon_{\Lambda_b^0}$ to be $\simeq 30\%$. Similarly, we vary the Peterson parameter ϵ between 0.002 and 0.010 for the Λ_b^0 and find the largest variation in $\epsilon_{B^0}/\epsilon_{\Lambda_b^0}$ to be $\simeq 17\%$. The uncertainty in the b-quark production cross section tends to cancel out in the ratio $\epsilon_{B^0}/\epsilon_{\Lambda_b^0}$ and therefore introduces a low systematic error. The same arguments apply to the other sources of systematic errors, which are listed in Table III.

Table III: Summary of the Systematic Uncertainties

Source of Uncertainty	Central Value Used in Analysis	Variation Range	Total Change in $\frac{\epsilon_{B^0}}{\epsilon_{\Lambda_b^0}}$, %
Λ_b^0 polarization	0	See Sec. 5.4	30
J/ψ helicity	0	-1 — 1	4
Peterson ϵ for Λ_b^0	0.006	0.002 — 0.010	17
Peterson ϵ for B^0	0.006	0.004 — 0.008	8
$c\tau(\Lambda_b^0), \mu$m	400	352 — 448	3
$c\tau(B^0), \mu$m	450	417 — 483	1
SVX $c\tau$ resolution, μm	50	40 — 60	1
J/ψ trigger efficiency in first 19.4 pb^{-1}	standard	$\pm 1\sigma$	5
J/ψ trigger efficiency in remainder of data	standard	$\pm 1\sigma$	2
b spectrum	$M_b = 4.75\ GeV/c^2$, $\mu = \mu_0$	$M_b = 4.5\ GeV/c^2$, $\mu = \mu_0/4$ to $M_b = 5.0\ GeV/c^2$, $\mu = 2 \times \mu_0$	2.5
Mass uncertainty scale parameter	1.15	0.9 — 1.7	5
Total Change			37

The various systematic errors are combined in quadrature to yield a maximum total variation in $\frac{\epsilon_{B^0}}{\epsilon_{\Lambda_b^0}}$ of 37%. We have treated this widest variation obtained as encompassing 90% of the possible range of systematic errors, corresponding to a range of approximately two standard deviations. Consequently, we quote 19% as a 1σ systematic uncertainty in the ratio of efficiencies.

5.5 Determination of $\frac{\sigma(p\overline{p}\to\Lambda_b^0 X)\mathcal{B}(\Lambda_b^0\to J/\psi\Lambda)}{\sigma(p\overline{p}\to B^0 X)\mathcal{B}(B^0\to J/\psi K_S^0)}$

Finally, for $P_T(\Lambda_b^0, B^0) > 6$ GeV/c, and $|\eta(\Lambda_b^0, B^0)| < 0.6$, we find for the ratio of cross section times branching fraction

$$\frac{\sigma(p\overline{p}\to\Lambda_b^0 X)\mathcal{B}(\Lambda_b^0\to J/\psi\Lambda)}{\sigma(p\overline{p}\to B^0 X)\mathcal{B}(B^0\to J/\psi K_S^0)} = 0.27 \pm 0.12(stat.) \pm 0.05(sys.).$$

6 Conclusions

The decay $\Lambda_b^0 \to J/\psi\Lambda$ has been observed. The Λ_b^0 mass is measured to be $5621 \pm 4(stat.) \pm 3(sys.)$ MeV/c^2. The mass difference with the B^0 is found to be $M_{\Lambda_b^0} - M_{B^0} = 340 \pm 5(stat.) \pm 1(sys.)$ MeV/c^2 . Several reference signals have been checked to confirm the calibration of this mass measurement.

The ratio of production cross section times branching fraction has been measured for the $\Lambda_b^0 \to J/\psi\Lambda$ and $B^0 \to J/\psi K_S^0$ decays and is found to be $\frac{\sigma_{\Lambda_b^0}\mathcal{B}(\Lambda_b^0\to J/\psi\Lambda)}{\sigma_{B^0}\mathcal{B}(B^0\to J/\psi K_S^0)} = 0.27 \pm 0.12(stat.) \pm 0.05(sys.)$. If we assume $\sigma_{\Lambda_b^0}/\sigma_{B^0} = 0.1/0.375$ and $\mathcal{B}(B^0 \to J/\psi K_S^0) = 3.7 \times 10^{-4}$, we find $\mathcal{B}(\Lambda_b^0 \to J/\psi\Lambda) = (3.7 \pm 1.7(stat.) \pm 0.7(sys.)) \times 10^{-4}$. This last value is in agreement with the CDF [4] and LEP limits [7, 21] and recent theoretical expectations [22]. The central value is approximately a factor 50 smaller than the central value of the UA1 result [3].

7 Acknowledgements

We thank the Fermilab staff and the technical staffs of the participating institutions for their vital contributions. This work was supported by the U.S. Department of Energy and National Science Foundation; the Italian Istituto Nazionale di Fisica Nucleare; the Ministry of Education, Science and Culture of Japan; the Natural Sciences and Engineering Research Council of Canada; the National Science Council of the Republic of China; and the A.P. Sloan Foundation.

References

[1] F. Abe *et al.*, Phys. Rev. Lett. **76**, 2015 (1996).
F. Abe *et al.*, Phys. Rev. Lett. **76**, 4462 (1996).
F. Abe *et al.*, "Measurement of the Lifetime of the B_s^0 Meson using the Exclusive Decay Mode $B_s^0 \to J/\psi\phi$.", FERMILAB-PUB-96-101-E, May 1996, submitted to Phys. Rev. Lett.

[2] W. Kwong and J. Rosner, Phys. Rev.D **44**, 212 (1991).

[3] C. Albajar *et al.*, Phys. Lett. B **273**, 540 (1991).

[4] F. Abe *et al.*, Phys. Rev. D **47**, 2639 (1993).

[5] F. Abe *et al.*, Phys. Rev. Lett. **77**, 1439 (1996).
D. Buskulic *et al.*, Phys. Lett. B **357**, 685 (1995).
P. Abreu *et al.*, Z. Phys. C **68**, 375 (1995).
R. Akers *et al.*, Z. Phys. C **69**, 195 (1996).

[6] D. Buskulic *et al.*, Phys. Lett. B **380**, 437 (1996).

[7] P. Abreu *et al.*, Phys. Lett. B **374**, 351 (1996).

[8] F. Abe *et al.*, Nucl. Instr. Meth. Phys. Res. **271**, 387 (1988).

[9] F. Abe *et al.*, Phys. Rev. D **50**, 2966 (1994).

[10] D. Amidei *et al.*, Nucl.Instr.Meth. Phys. Res., Sect. A, **350**, 73 (1994).

[11] Particle Data Group, Phys. Rev. D **54**, 1 (1996).

[12] F. Abe *et al.*, Phys. Rev. Lett. **71**, 1686 (1993).

[13] F. Abe *et al.*, Phys. Rev. D **53**, 3496 (1996).

[14] F. Abe *et al.*, Phys. Rev. D **52**, 4784 (1995).

[15] F. Abe *et al.*, Phys. Rev. D **53**, 1051 (1996).

[16] P. Nason, S. Dawson, and R.K. Ellis, Nucl. Phys. **B327**, 49 (1989).

[17] A.D. Martin, W.J. Stirling, and R.G. Roberts, Phys. Rev. D **47**, 867 (1993).

[18] C. Peterson *et al.*, Phys. Rev. D **27**, 105 (1983).

[19] A. Fridman *et al.*, CERN-PPE-93-61.

[20] J.G. Korner *et al.*, Phys. Lett. B **275**, 495 (1992).

[21] F. Pierre,"New B States (B_s^0, Λ_b^0, Ξ_b...)", Proceedings of the Fifth International Symposium on Heavy Flavour Physics, Montreal, Canada, 1993

[22] H. Cheng *et al.*, IP-ASTP-22-94.

Figure Captions

1. The $\mu^+\mu^-$ invariant mass distribution. The shaded distribution contains events that satisfied a $P(\chi^2) > 0.005$ cut on the vertex and mass constrained fit to the world average J/ψ mass. These events are used in the exclusive reconstruction.

2. The J/ψ flight distance uncertainty distribution. The calculated uncertainty on the transverse flight distance of the J/ψ candidate in the direction of its momentum is shown. Events below a cut of 250 μm (indicated by the arrow) are used for the branching fraction measurement. The peak below 250 μm is from those events where both muons are measured in the SVX system.

3. The $\pi^+\pi^-$ invariant mass distribution. The area between the arrows indicates the combinations used as K^0_S candidates.

4. The $\pi^- p$ invariant mass distribution. The area between the arrows indicates the combinations used as Λ candidates.

5. The $J/\psi\pi^+\pi^-$ invariant mass distribution used for the $\psi(2S)$ mass measurement.

6. The $J/\psi\gamma$ invariant mass distribution used for the $\chi_{c1}(1P)/\chi_{c2}(1P)$ mass measurement.

7. The $\Lambda\pi^-$ invariant mass distribution used for the Ξ^- mass measurement. (A) The mass distribution for all both charge combinations. The solid line histogram is for events where both pions in the final state have the same charge. The dashed line corresponds to events where the pions have opposite charge. (B) The $\Lambda\pi^-$ spectrum. (C) The $\bar{\Lambda}\pi^+$ spectrum.

8. The $J/\psi K^0_S$ invariant mass distribution used for the B^0 mass measurement.

9. The $J/\psi\Lambda$ invariant mass distribution used for the Λ^0_b mass measurement. The curve is the result of a binned fit with the width of the Gaussian signal fixed at 13 MeV/c^2. In the 4 consecutive bins with the highest number of events we observe 35 events. In the 5 bins in the mass range $5.60 - 5.65$ GeV/c^2 we observe 38 events on a background of 18.1 events.

10. The P_T distribution of pions in the Λ signal region. The solid line indicates the P_T distribution of pions in the Λ signal region, while the dashed distribution covers the sidebands with $\pi^- p$ mass in the ranges $1107.6 - 1111.6$ or $1119.6 - 1123.6$ MeV/c^2. The arrow indicates the 400 MeV/c cut used for the rate measurement.

11. The number of K^0_S candidates with $P_T(K^0_S) > 2.0$ GeV/c versus the cosine of the decay angle. The distribution is relatively flat until large values of the decay angle are reached ($|\cos(\Theta)| > 0.7$). The decline corresponds to decays in which one of the π from the K^0_S has a transverse momentum below 400 MeV/c.

12. Λ^0_b and B^0 candidates used for the measurement of $\sigma_{\Lambda^0_b}\mathcal{B}(\Lambda^0_b \to J/\psi\Lambda)$. The additional cuts applied on the data are explained in the text.

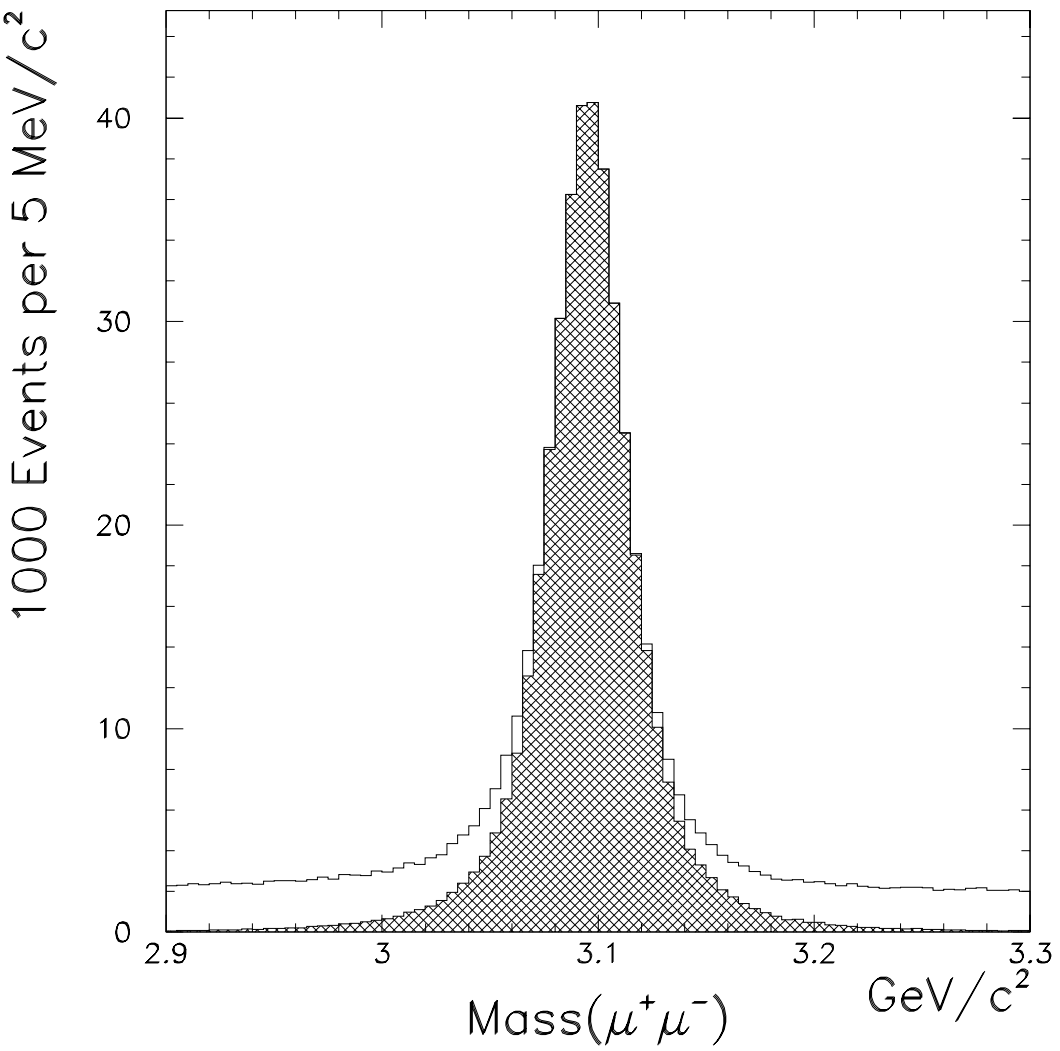

Figure 1:

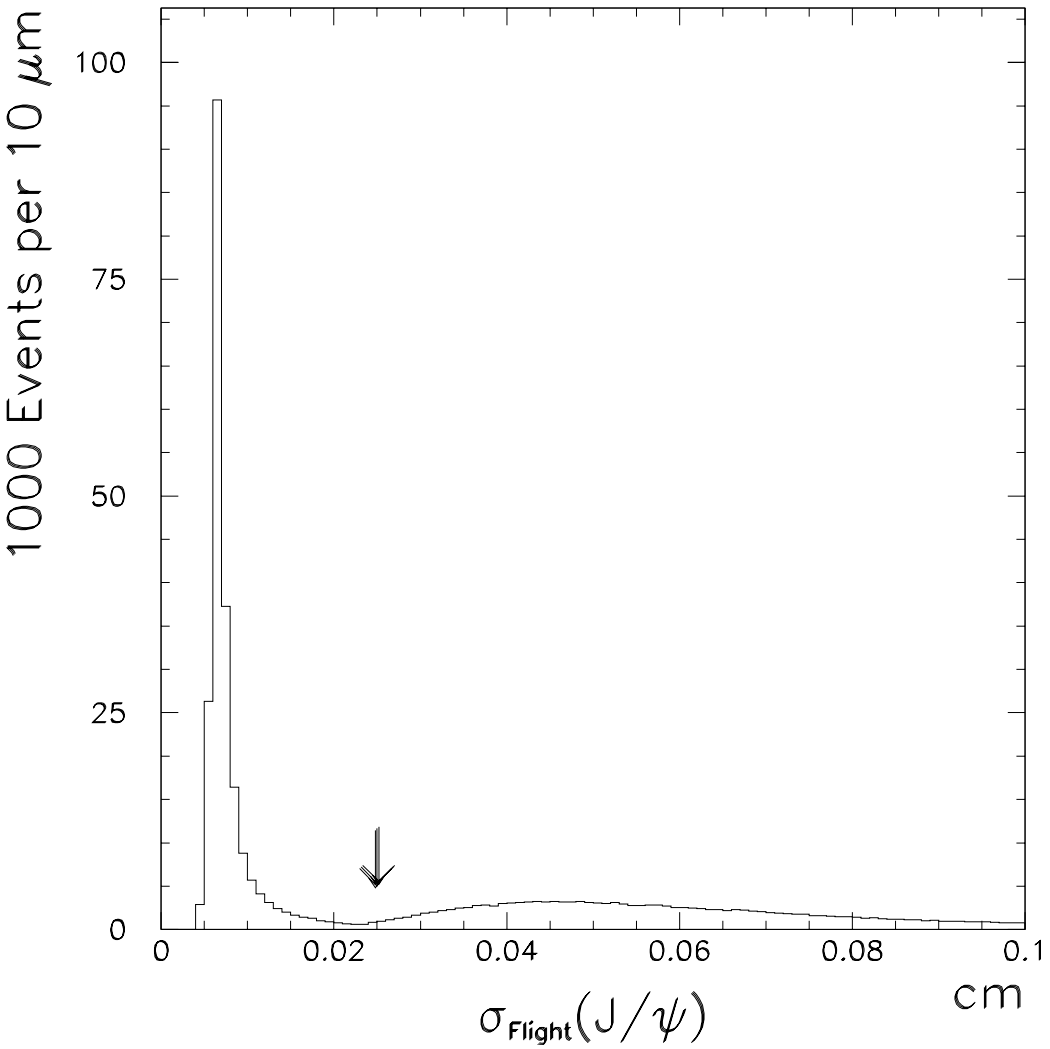
1000 Events per 10 μm
100
75
50
25
0
0
0.02
0.04
0.06
0.08
0.1
cm
$\sigma_{\text{Flight}}(J/\psi)$

Figure 2:

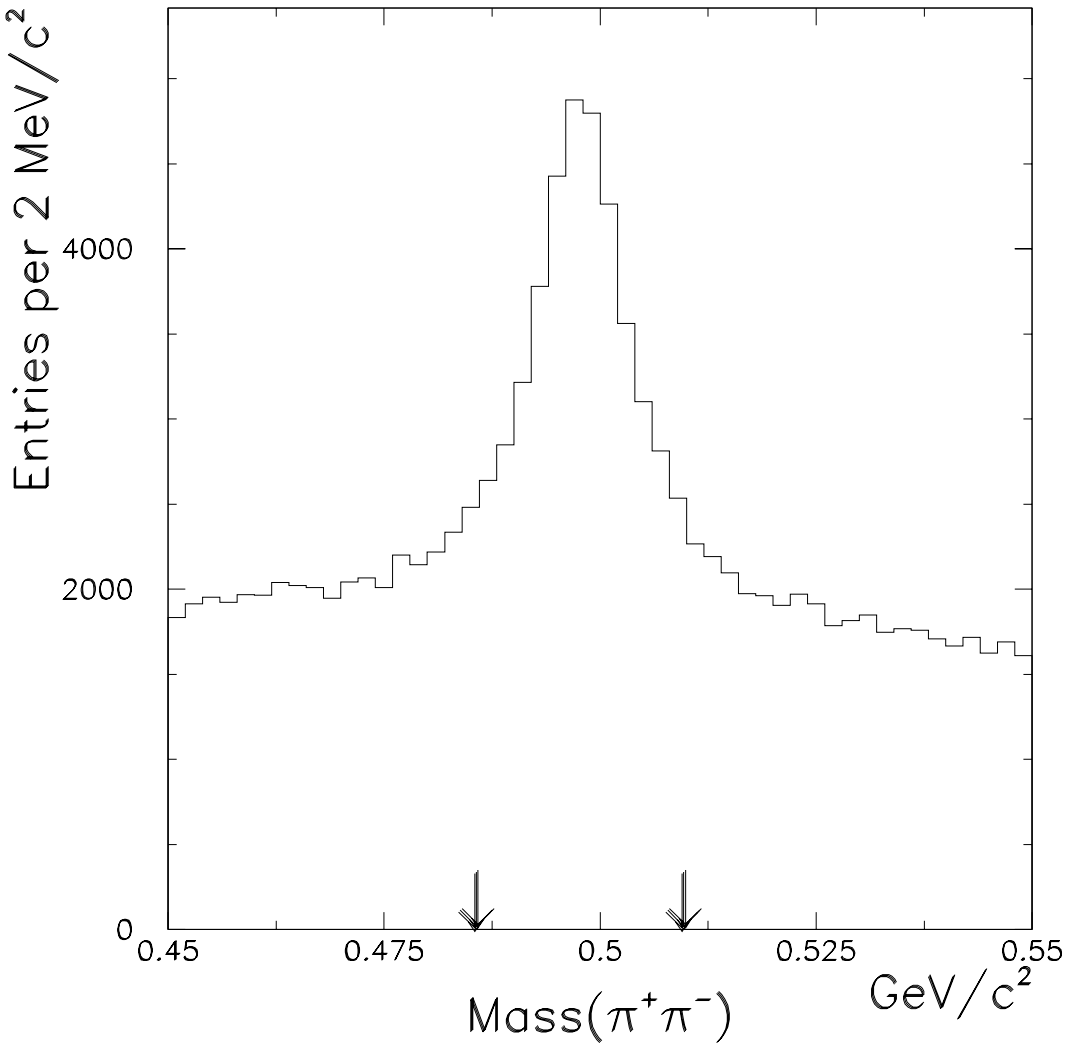
Entries per 2 MeV/c²
4000
2000
0
0.45
0.475
0.5
0.525
0.55
Mass(π⁺π⁻)
GeV/c²

Figure 3:

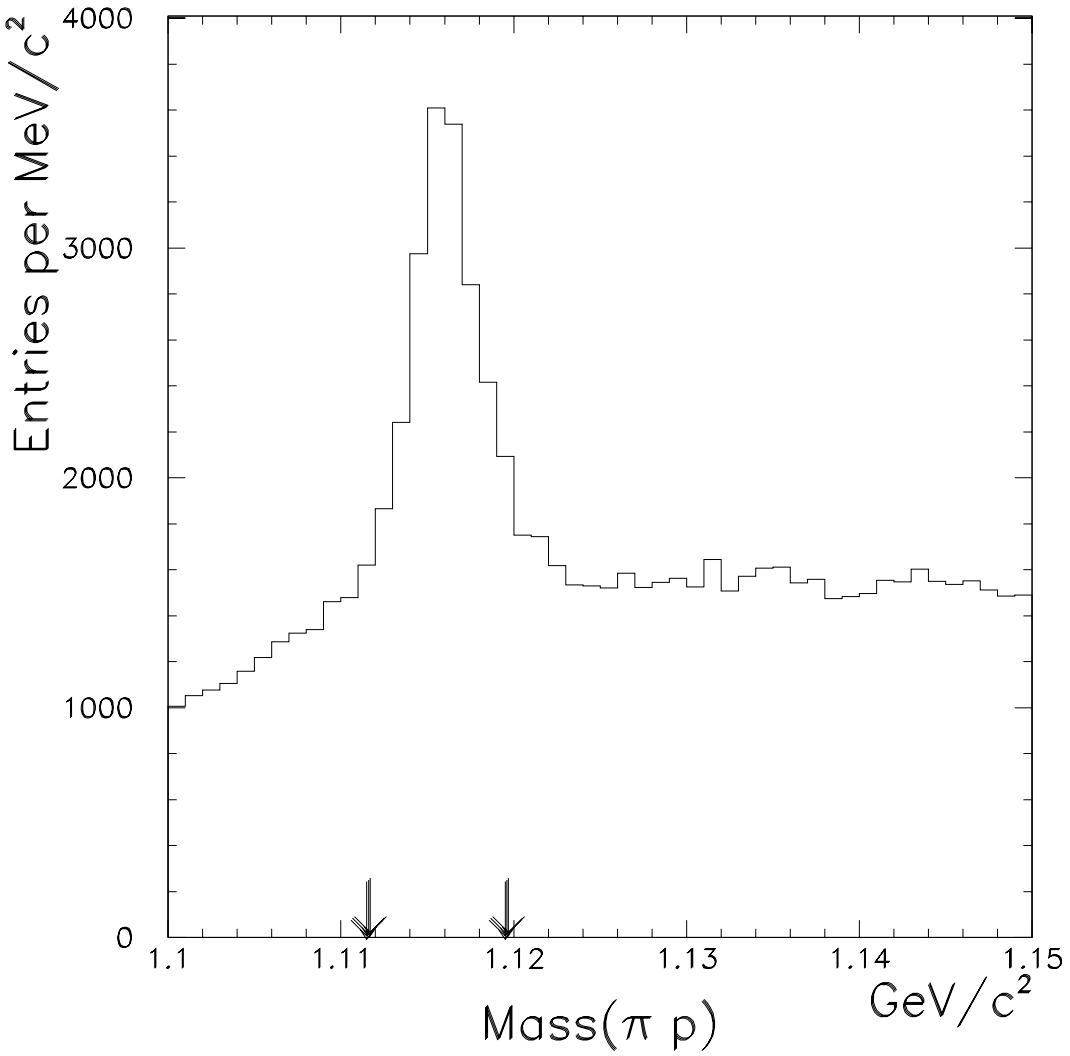
Entries per MeV/c²
4000
3000
2000
1000
0
1.1
1.11
1.12
1.13
1.14
1.15
Mass(π p)
GeV/c²

Figure 4:

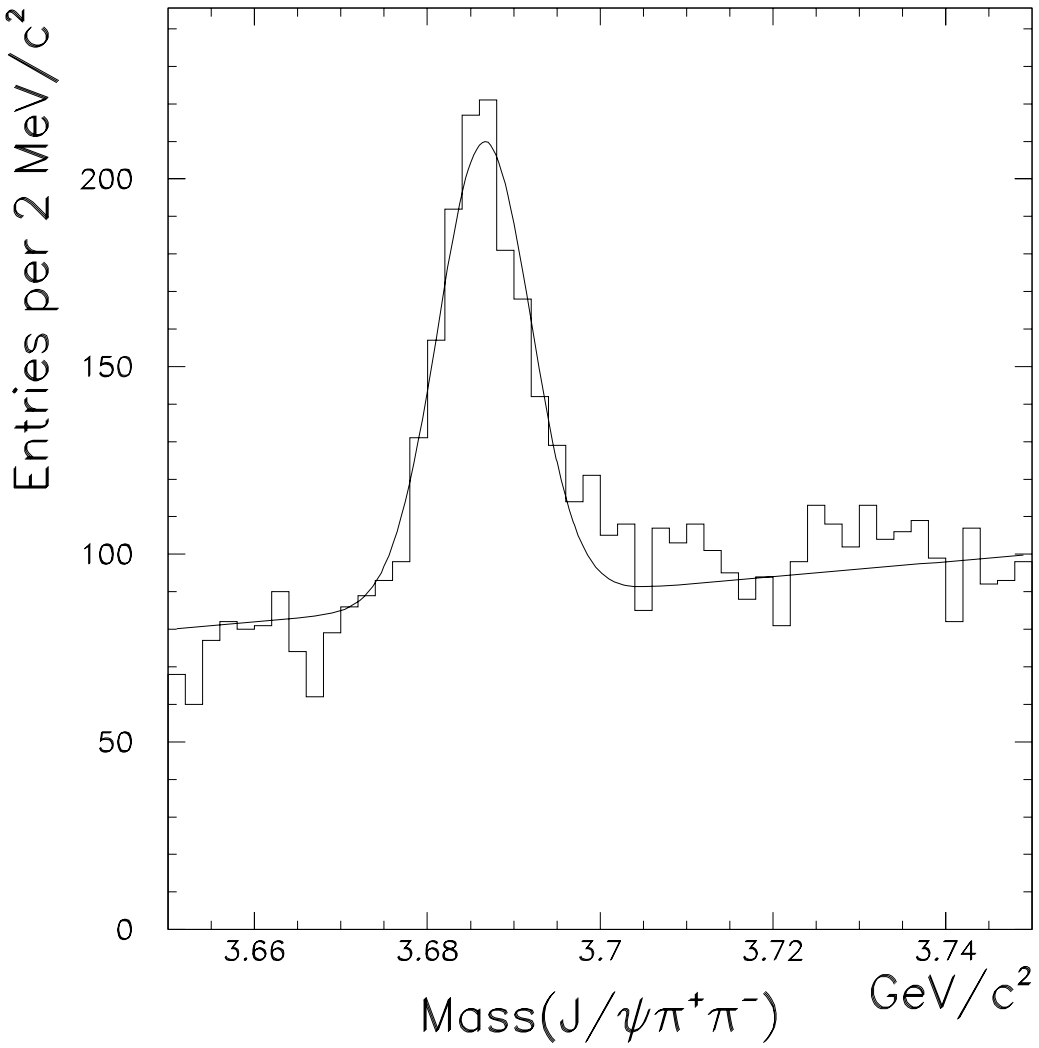
Entries per 2 MeV/c²
200
150
100
50
0
3.66
3.68
3.7
3.72
3.74
Mass(J/ψπ⁺π⁻)
GeV/c²

Figure 5:

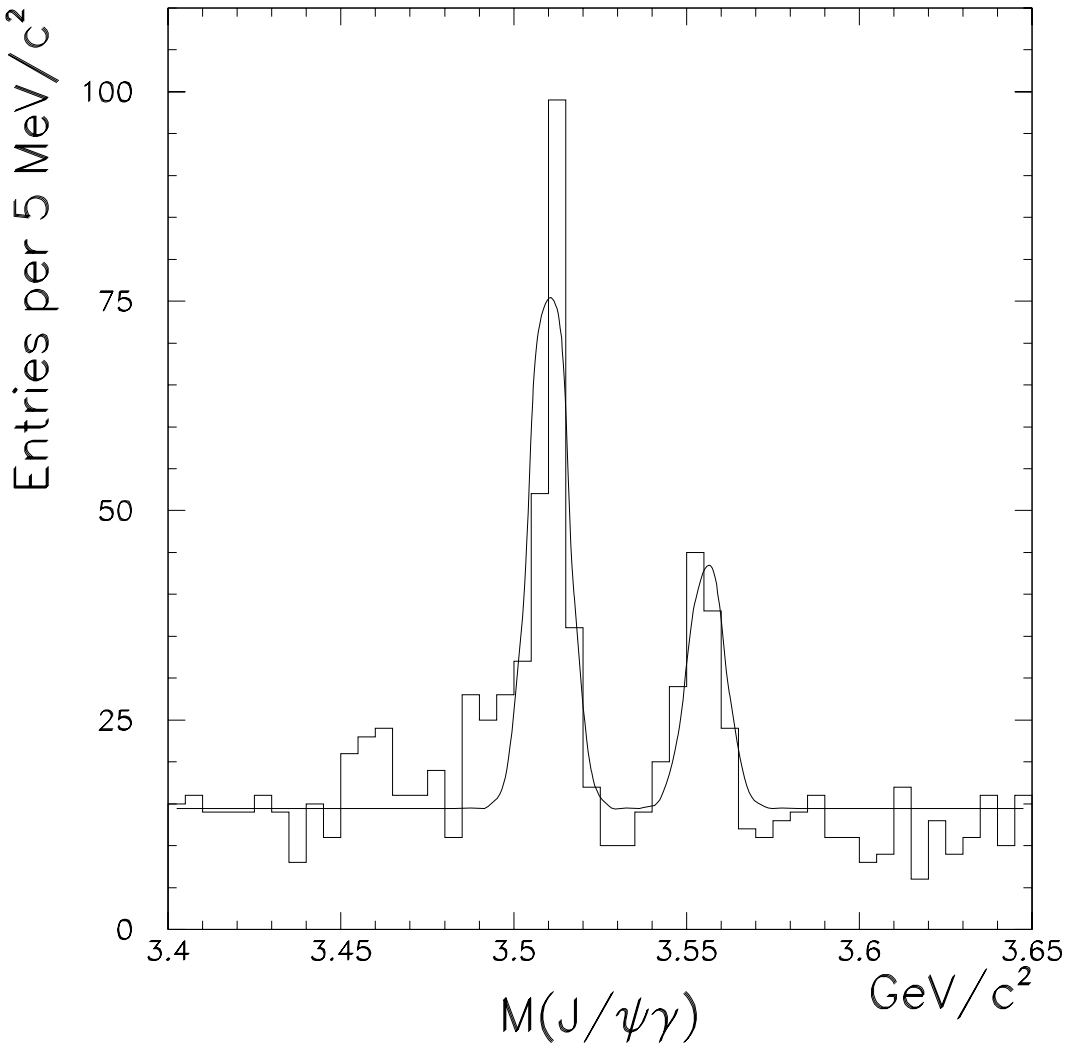
Entries per 5 MeV/c²
100
75
50
25
0
3.4
3.45
3.5
3.55
3.6
3.65
M(J/ψγ)
GeV/c²

Figure 6:

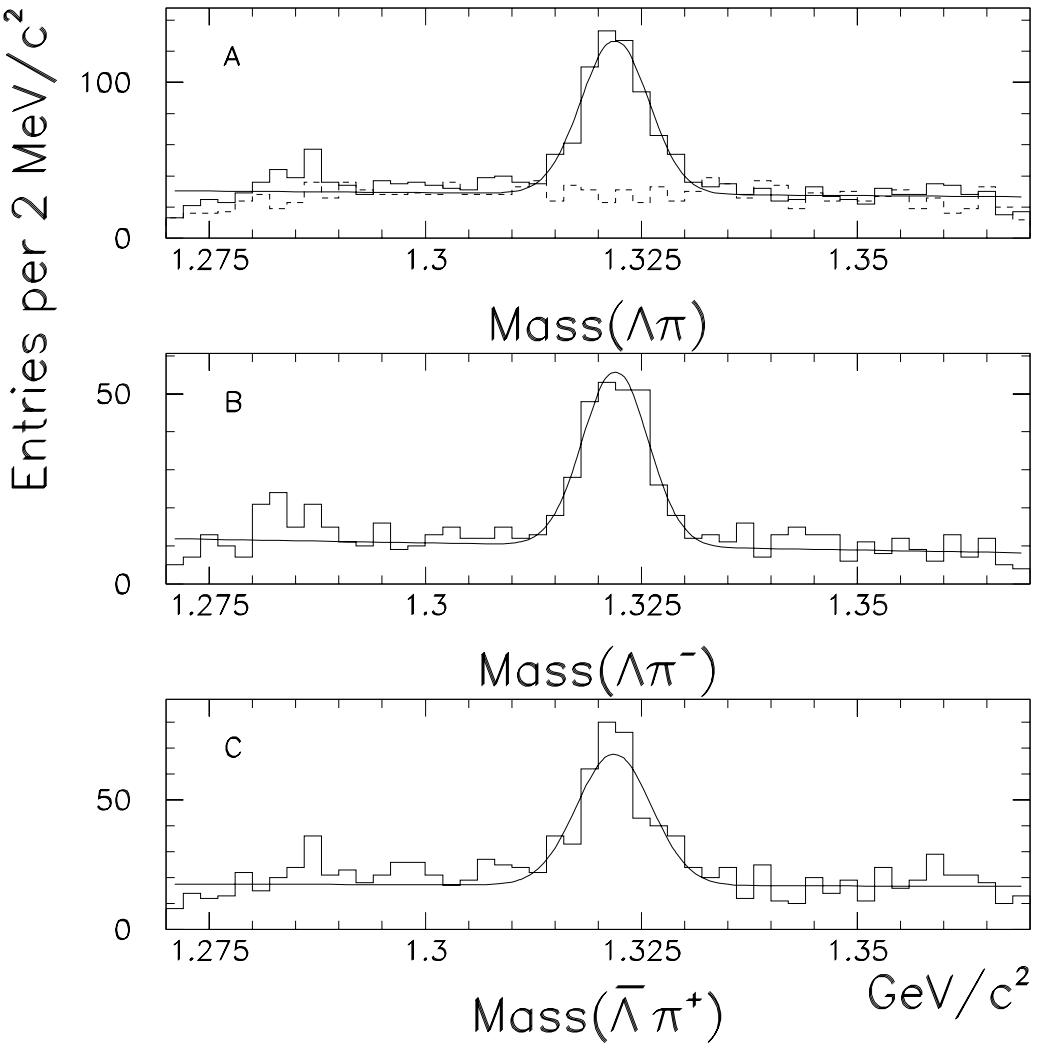
Entries per 2 MeV/c²
A
100
0
1.275
1.3
1.325
1.35
Mass(Λπ)
B
50
0
Mass(Λπ⁻)
C
50
0
Mass(Λ̄π⁺)
GeV/c²

Figure 7:

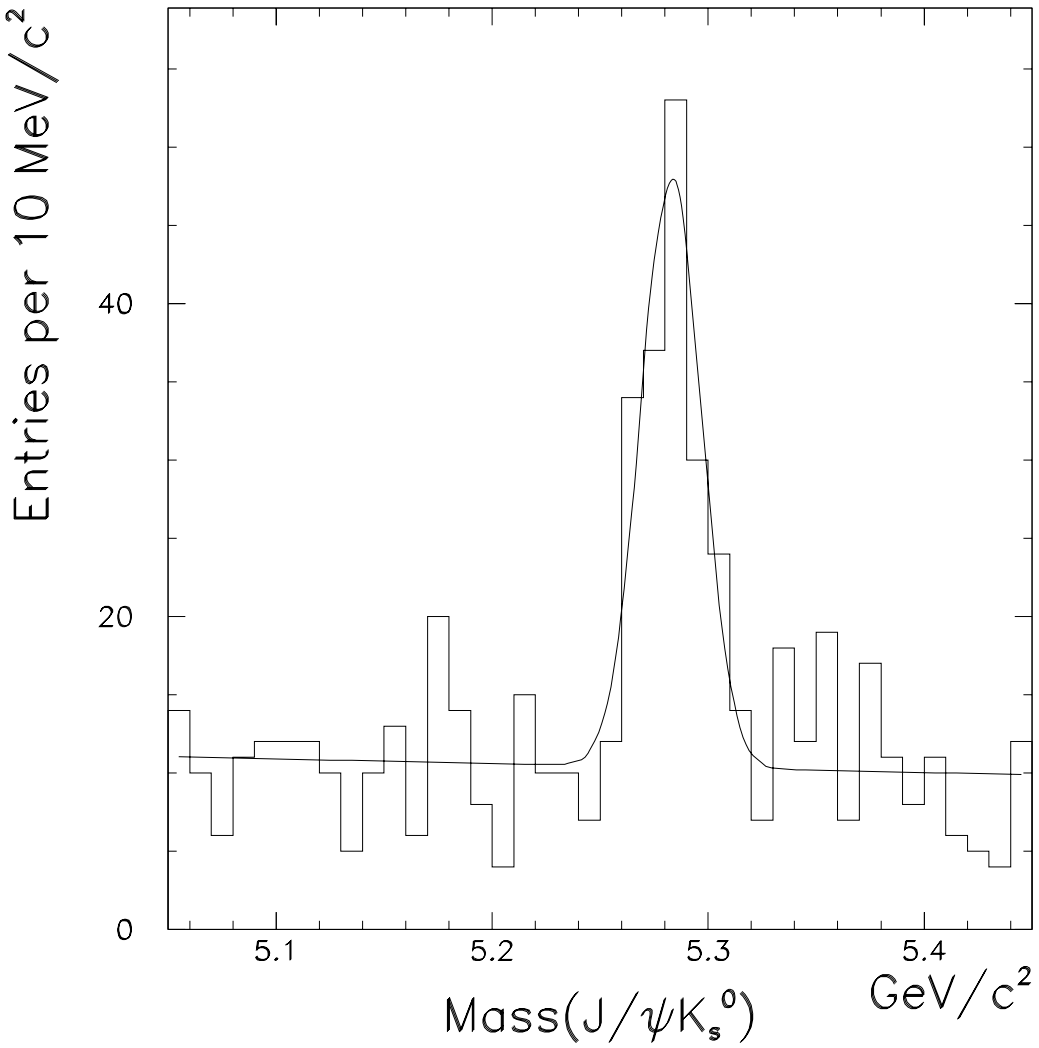

Figure 8:

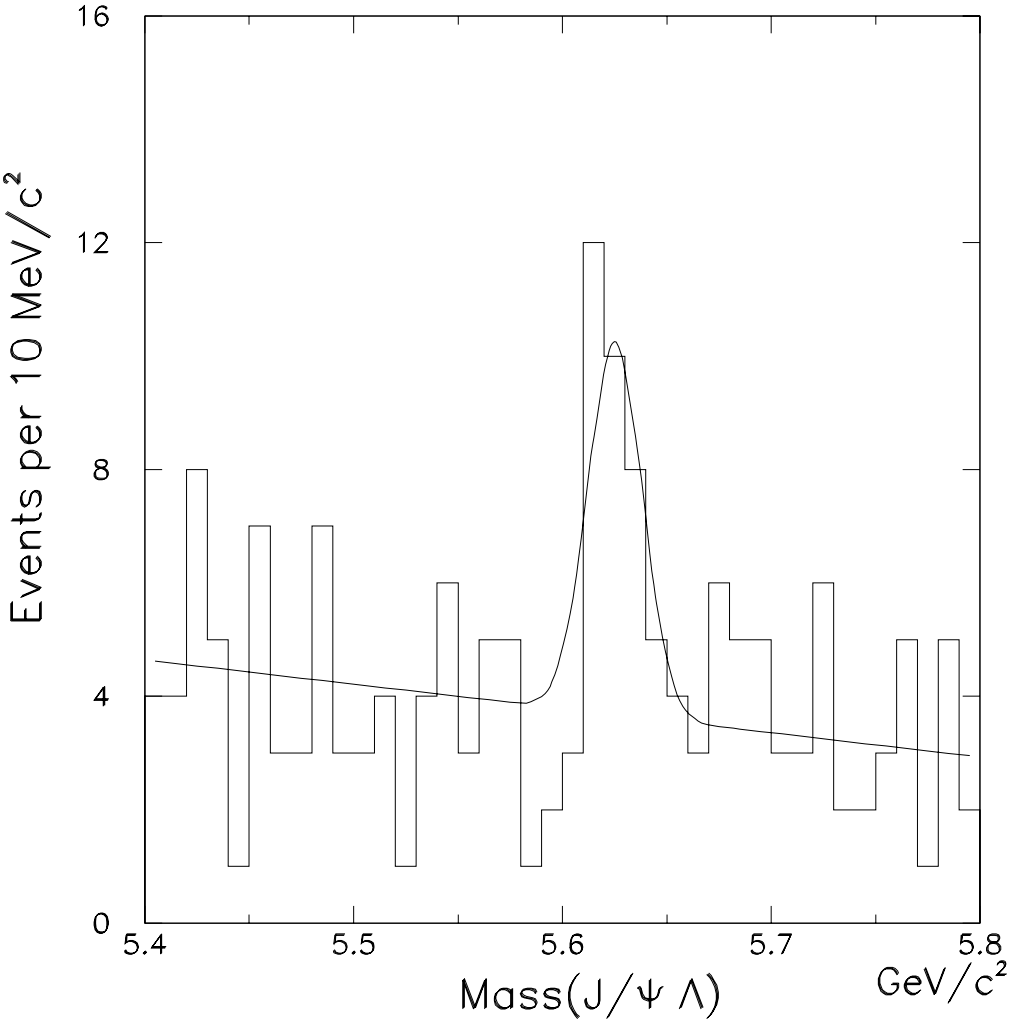

Figure 9:

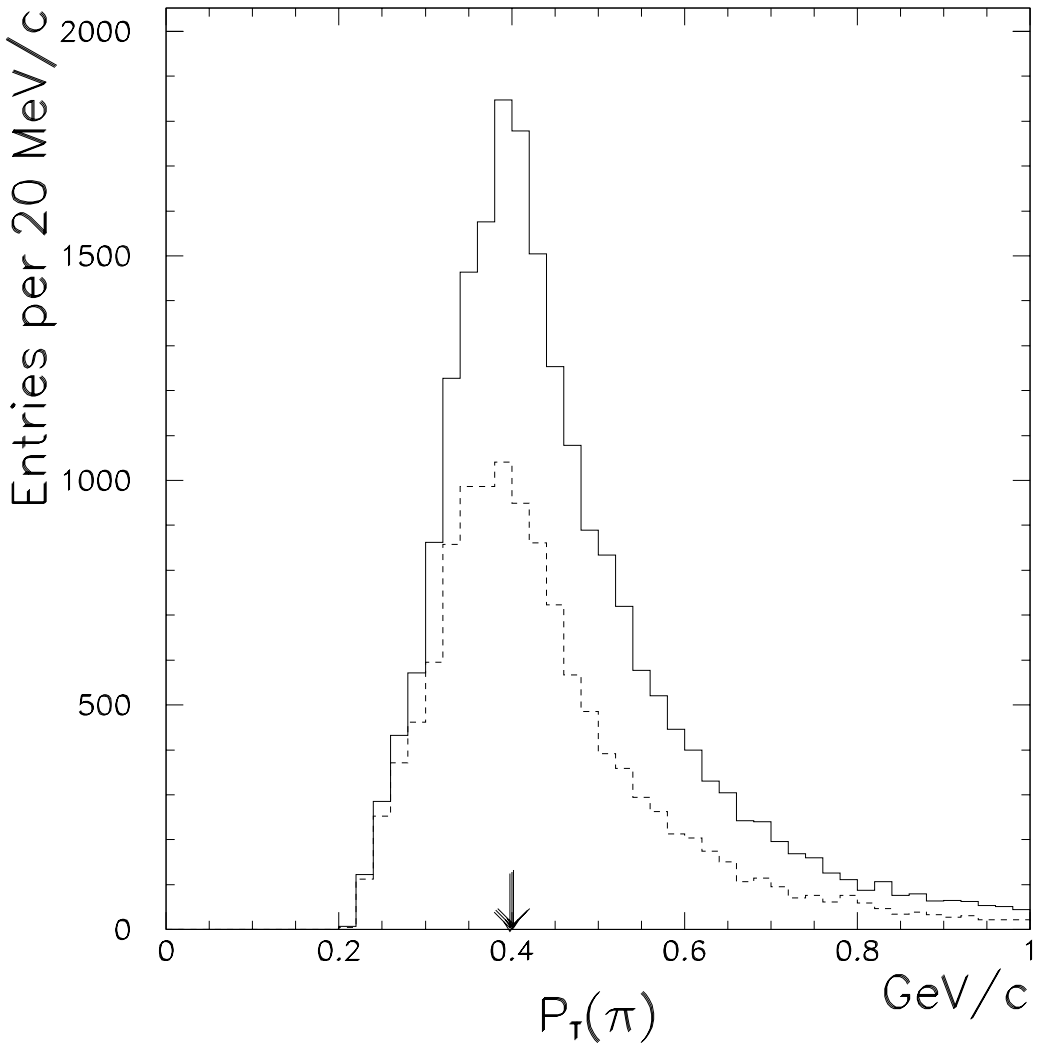
Entries per 20 MeV/c
2000
1500
1000
500
0
0
0.2
0.4
0.6
0.8
1
$P_T(\pi)$
GeV/c

Figure 10:

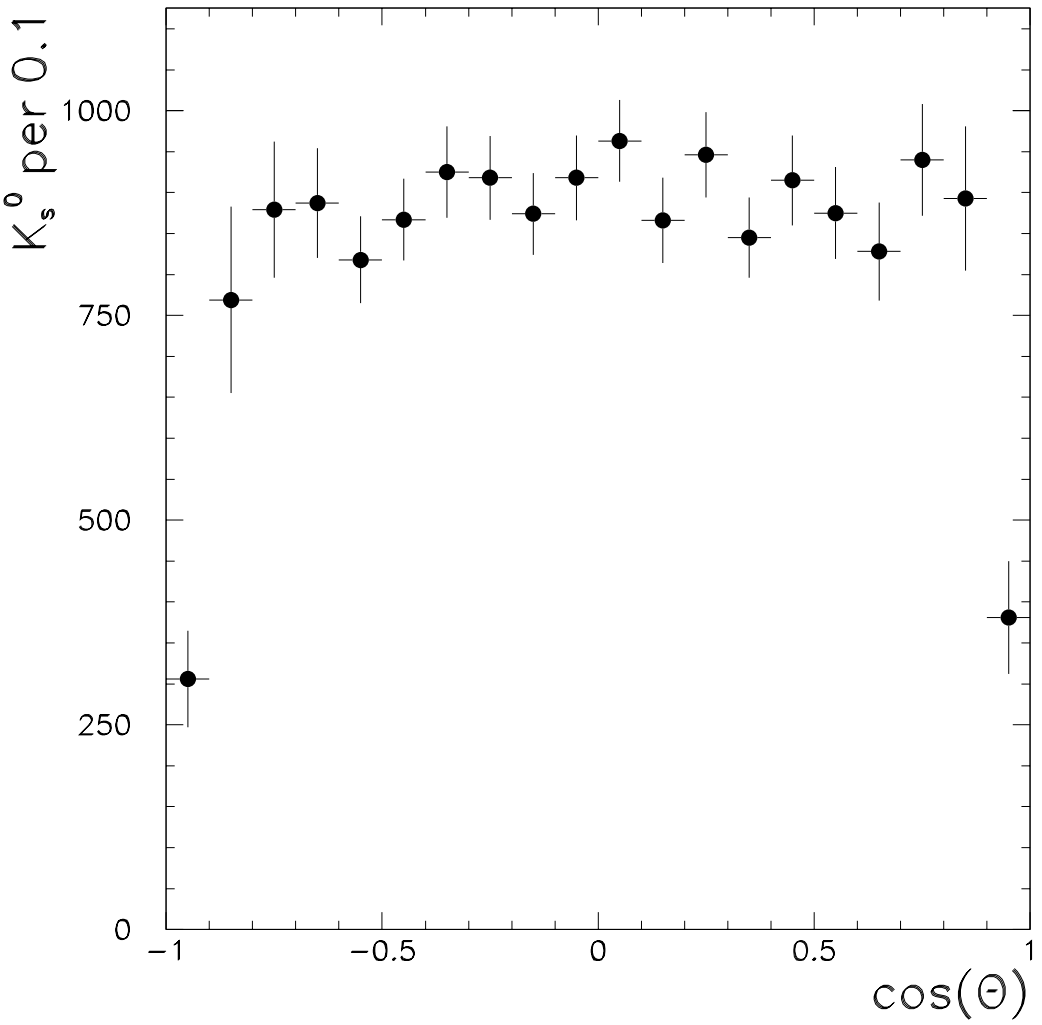

Figure 11:

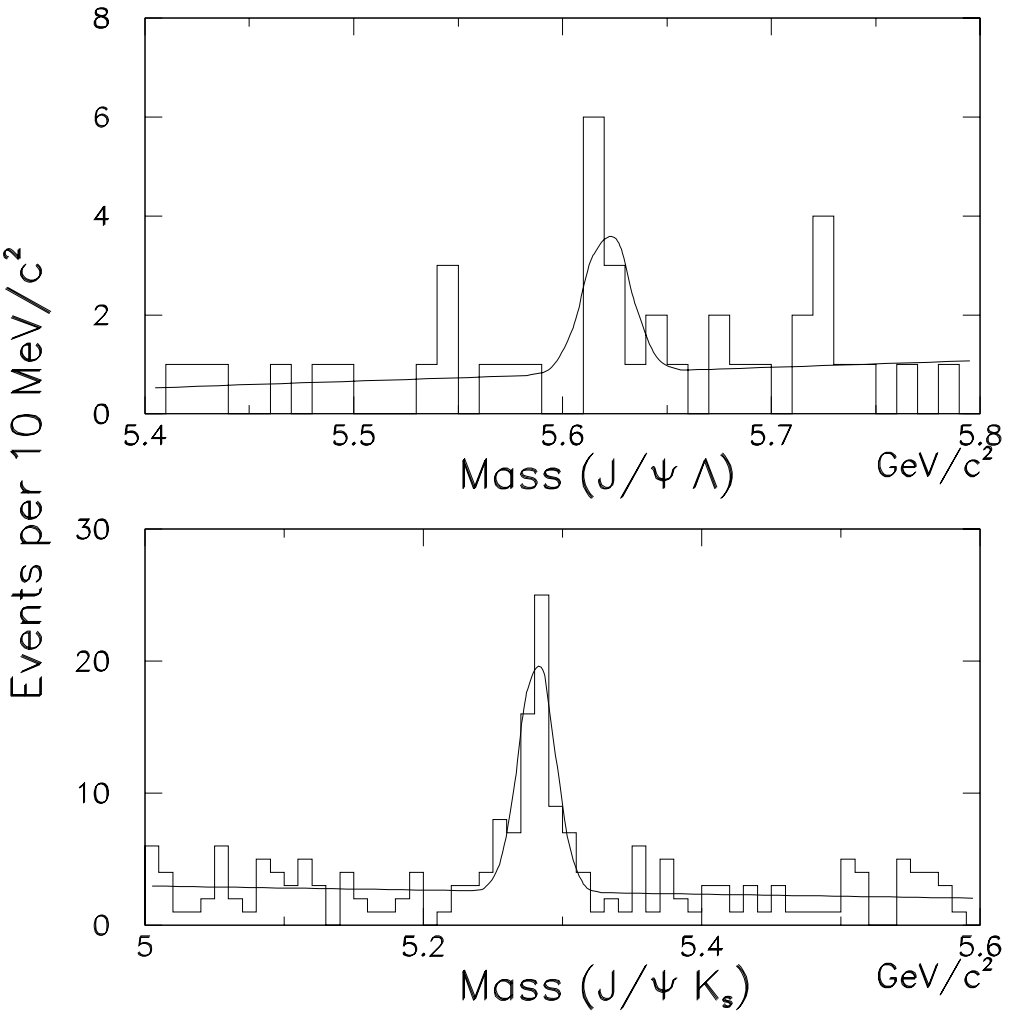
Events per 10 MeV/c²
8
6
4
2
0
5.4
5.5
5.6
5.7
5.8
Mass (J/ψ Λ)
GeV/c²
30
20
10
0
5
5.2
5.4
5.6
Mass (J/ψ K_s)
GeV/c²

Figure 12: